Computational and Theoretical Chemistry 987 (2012) 77–83

Contents lists available at ScienceDirect

Computational and Theoretical Chemistry

journal homepage: www.elsevier.com/locate/comptc

CO adsorption on Pt (1 1 1) and Pd (1 1 1) surfaces: A first-principles based lattice gas Monte-Carlo study

R. Chen [a,b], Z. Chen [c], B. Ma [c], X. Hao [d], N. Kapur [d], J. Hyun [d], K. Cho [e,*], B. Shan [f,c,**]

[a] State Key Laboratory of Digital Manufacturing Equipment and Technology, Huazhong University of Science and Technology, Wuhan 430074, Hubei, China
[b] Department of Mechanical Engineering, Huazhong University of Science and Technology, Wuhan 430074, Hubei, China
[c] Department of Materials Science and Engineering, Huazhong University of Science and Technology, Wuhan 430074, Hubei, China
[d] Nanostellar Inc., 3696 Haven Ave., Redwood City, CA 94063, USA
[e] Department of Materials Science and Engineering, The University of Texas at Dallas, Richardson, TX, USA
[f] State Key Laboratory of Material Processing and Die & Mould Technology, Huazhong University of Science and Technology, Wuhan 430074, Hubei, China

ARTICLE INFO

Article history:
Received 4 February 2011
Received in revised form 23 May 2011
Accepted 15 July 2011
Available online 26 July 2011

Keywords:
CO adsorption
Monte-Carlo
Lattice gas
First-principles

ABSTRACT

Interaction of carbon monoxide (CO) with transition metal surfaces is an essential part of CO oxidation catalysis. In this report, we investigate and compare CO adsorption behavior on Pt (1 1 1) and Pd (1 1 1) surfaces combining first-principles (FP) calculations and lattice gas Monte-Carlo (LG-MC) simulations. Our results indicate that despite stronger CO binding on Pd (1 1 1) at low coverage, more repulsive lateral interactions on Pd surface lead to a more rapid adsorption energy decrease with respect to coverage. This results in lower saturation coverage and weaker CO desorption energies on Pd (1 1 1), which could contribute to its excellent reactivity observed under high pressure reaction conditions.

1. Introduction

Vehicle emission control standards necessitate the development of highly efficient carbon monoxide (CO) oxidation catalysts for the removal of CO from engine exhausts via oxidation reaction. Platinum group metals (PGM), especially platinum (Pt) and palladium (Pd) are among the most widely used transition metal catalysts for diesel exhaust aftertreatment [1,2]. Well dispersed platinum nanoparticles catalyze CO oxidation reaction at low temperatures, and show a very robust performance under realistic high pressure diesel engine operating conditions [3–6]. One of the obstacles with the application of Pd nanoparticles as practical CO oxidation catalysts is their tendency towards bulk oxide formation and the accompanying irreversible loss of reactivity. Progress in the stabilization of Pd metal has been made via alloying with other noble metals such as gold [7,8].

It is generally accepted that CO oxidation on PGM surfaces proceeds via Langmuir–Hinshelwood (LH) mechanism [9,10], which involves CO adsorption and its subsequent reaction with dissociated atomic oxygen to form CO_2. In real-life operation of diesel engine catalytic converters, the CO oxidation reaction takes place under high gas pressure, and reaction kinetic analysis shows that the transition metal surface is inhibited by adsorbed CO molecules at the onset of oxidation, and that the rate determining step in the oxidation reaction could be the CO desorption from the surface [11,12]. Due to the importance of CO adsorption/desorption processes in the overall reaction, many experimental techniques, including thermal desorption spectroscopy (TPD) [13], low energy electron diffraction (LEED) [14,15], electron energy loss spectroscopy (EELS) [16], and scanning tunneling microscopy (STM) [17,18], have been used to probe the CO adsorption behavior on transition metal surfaces. However, despite many valuable insights gained from these experimental investigations, there is still a lack of understanding on detailed CO molecular interactions on transition metal surfaces. On the theoretical side, though important information about adsorption behaviors of CO on a Pt (1 1 1) surface in low coverage limits was reported [19,20], there have only been a limited number of theoretical studies addressing the CO adsorption at high coverage, which is in part due to the complex nature of CO lateral interactions that can stabilize CO molecules into quite different adsorption configurations. Some previous studies either used a manually generated set of adsorption configurations [21], or used an average effective lateral interaction between CO molecules [22], which might lead to inaccuracies. To the best of our knowledge, we are not aware of a systematic, comparative theoretical study that deals with high coverage CO adsorption on both Pt (1 1 1) and Pd (1 1 1) surfaces.

* Co-Corresponding author.
** Corresponding author at: Department of Materials Science and Engineering, Huazhong University of Science and Technology, Wuhan 430074, Hubei, China.
E-mail addresses: kjcho@utdallas.edu (K. Cho), bshan@mail.hust.edu.cn (B. Shan).

2210-271X/$ - see front matter © 2011 Elsevier B.V. All rights reserved.
doi:10.1016/j.comptc.2011.07.015

An understanding of CO adsorption at high coverage is nonetheless of great importance in the development and improvement of transition metal CO oxidation catalysts. The CO saturation coverage and adsorption pattern influence both the CO desorption energy [22] and the oxygen dissociation barrier on the surface [23], two most important steps in the CO oxidation via LH mechanism [24]. In this study, we report the simulation results of CO adsorption on Pt (1 1 1) and Pd (1 1 1) surfaces from first-principles (FP) based lattice gas Monte-Carlo (LG-MC) simulations. The LG parameters were obtained from an extensive set of FP density functional theory (DFT) calculations. Our simulations show that though CO binds stronger on Pd (1 1 1) at low coverage, the substrate-mediated lateral interaction via metal sharing leads to a more rapid CO adsorption energy decrease on Pd (1 1 1) as coverage increases. Beyond a crossing point around 0.50 monolayer (ML), CO adsorption energy becomes weaker on Pd (1 1 1) than that on Pt (1 1 1). The predicted CO saturation coverage on Pt (1 1 1) and Pd (1 1 1) are ~0.75 ML and ~0.70 ML, respectively. Lower CO desorption energies at high coverage on Pd (1 1 1) could be one of the key factors that contribute to the excellent performance of Pd and Pd-based alloys in CO oxidation catalysis [7,25].

2. Computational methods

We used state-of-the-art FP-DFT total energy calculations to evaluate self-consistently all the CO interaction parameters needed for the LG-MC simulations. The DFT calculations were done using the Vienna Ab-initio Simulation Package (VASP) [26], where Kohn–Sham single-electron wavefunctions were expanded by plane waves with an energy cutoff of 400 eV. This ensures the convergence of CO adsorption energies to a few millivolts. The interactions between ions and valence electrons were described using the projected augmented wave (PAW) method [27]. We have calculated the adsorption energy per CO molecule on Pt (1 1 1) at 25% coverage with different exchange–correlation functionals and found Revised Perdew-Burke-Erzernhof (RPBE) [28] functional presented the closest value to experiments [14,29] and was used throughout all calculations. It is known that standard DFT underestimates the HOMO–LUMO gap of an adsorbed CO molecule and stabilizes threefold adsorption on Pt (1 1 1), in contradiction to experimental measurements [30,31]. Some theoretical works have proposed the use of different exchange–correlation functionals or additional empirical correction terms to remedy the site preference problem [30,32]. However, firstly, intrinsic adsorption energy differences are small as compared to lateral interactions at high coverage (shown in Section 3.1). Secondly, since it is not the primary focus of the current paper to discuss the effects of different functionals on low coverage CO adsorption energies, and to achieve an unbiased comparison between Pt and Pd, we used DFT adsorption energies without additional corrections [33,22]. The metal substrate was modeled by a three-layer slab separated by a vacuum layer thickness of approximately 15 Å, with atoms in the first two layers free to relax and those in the bottom layer fixed in their crystallographic locations. The whole system was allowed to relax until the Hellman–Feynman force on each atom is less than 0.03 eV/Å[22,23,34]. The CO adsorption energies were calculated as the total energy difference between the optimized (metal slab)–CO complex and the sum of the energies of the optimized bare slab and gas phase CO molecules:

$$E_{ads} = E_{\text{total}} - (E_{slab} + n \cdot E_{\text{CO}}), \tag{1}$$

where E_{total} and E_{slab} refer to the total system energy and slab energy, respectively. n is the number of adsorbed CO molecules. A total of 94 configurations of CO adsorption on Pt (1 1 1) and Pd (1 1 1) were calculated to parameterize the CO on-site adsorption energies and lateral interactions for the LG-MC simulation. These configurations were chosen to have reasonable intermolecular CO distances and span a reasonable configuration space in LG parameters. The geometries of these configurations are not shown here for brevity, but are similar to the ones used in a previous study [22]. The LG-MC simulation was then used to explore CO adsorption configurations beyond the DFT adsorption patterns [35,36] that are usually limited to a small unit cell. The LG model has previously been successfully applied to the calculation of phase diagrams for a large number of alloy systems and surfaces [35,37]. In this model, the total energy is expressed as

$$E_{ads}(\sigma_1, \sigma_2, \ldots, \sigma_N) = V_0 + \sum_i V_i \sigma_i + \frac{1}{2} \sum_{i,j} V_{ij} \sigma_i \sigma_j + \frac{1}{6} \times \sum_{i,j,k} V_{ijk} \sigma_i \sigma_j \sigma_k + \cdots, \tag{2}$$

where V_0 is a constant, and set to zero without loosing of generality. σ_i represent site occupation numbers of different sites, and V_i is the corresponding on-site adsorption energy. V_{ij} and V_{ijk} correspond to two-body interactions and three-body interactions, respectively. The coefficients were obtained via a least square fit of LG model to DFT energies. Since the diffusion barriers of molecularly adsorbed CO are small compared to other elementary steps, we can assume that the adlayer on metal surfaces under normal situations are equilibrated [37]. The Monte-Carlo technique with Metropolis algorithm [38] was used to equilibrate the adsorption on surface and to evaluate the energy of equilibrated CO adsorption on a topologically fixed underlying lattice. At each coverage, we deposited an initial random distribution of CO molecules on the surface and allowed the adsorbed CO molecules to change their positions. All trial moves were either accepted or rejected according to the basic Metropolis scheme. Since many of the experimental CO adsorption characterization works were carried out under low temperatures, we set the equilibrium temperature to 70 K. Simulated annealing technique has been used to ensure the sampling of adequate part of the whole phase space in MC simulations [39]. We started with 2570 K, and decreased the temperature by 50 K after every 100 MC pass (1 MC pass is defined as one flip per adsorption site on average) until it reaches 70 K. An additional 10^8 MC steps following the annealing process is used to equilibrate the system. For a given coverage, the aforementioned processes were repeated 10 times to make sure the system was adequately equilibrated.

3. Results and discussions

3.1. Low coverage CO adsorption

We first discuss the adsorption of CO molecules under low coverage conditions. On both Pt (1 1 1) and Pd (1 1 1) surfaces, there are four types of stable binding sites (Atop, Bridge, Fcc, Hcp), as indicated on Fig. 1a. E_{ads}s of CO on the Pt (1 1 1) surface at 0.06 ML [corresponding to one molecular CO adsorption in a $p(4 \times 4)$ unit cell] are 1.52 (A), 1.59 (B), 1.60 (F), 1.57 (H) eV, respectively. Fcc sites are predicted as the most stable adsorption sites. The discrepancy between DFT calculations and experimental observations has been discussed in Section 2. On the Pd (1 1 1) surface, the CO adsorption energies are 1.17 (A), 1.57 (B), 1.72 (F), and 1.72 (H) eV for the same four types of sites, with fcc and hcp sites being most stable and almost isoenergetic. Fig. 1b and c show contour plots of CO adsorption energies on Pt (1 1 1) and Pd (1 1 1), respectively. Clearly, the corrugation is much stronger on Pd (1 1 1), due to the relatively larger adsorption energy difference between atop and threefold sites. In both cases, the diffusion barrier of CO on the surface is small compared to CO oxidation barrier of around 1.0 eV [40,41]. Thus we conclude that under low coverage condi-

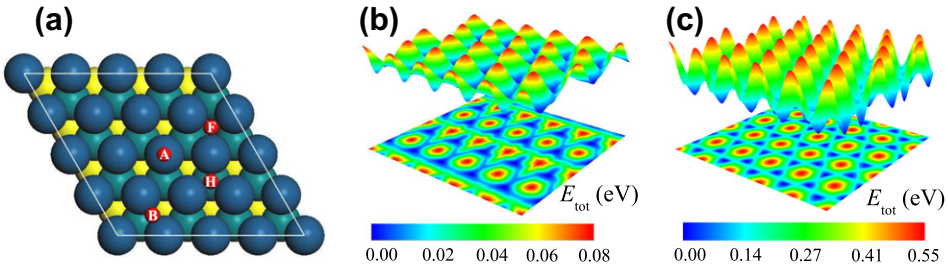

Fig. 1. (a) Stable CO adsorption hcp (H), fcc (F), atop (A), and bridge (B) sites on Pt (1 1 1) and Pd (1 1 1), shown as small red spheres. Darkblue and lightblue spheres represent surface and sub surface atoms, respectively. White dotted line indicates the $p(4 \times 4)$ unit cell for DFT adsorption calculations. (b) Adsorption energy contour for CO on the Pt (1 1 1) surface. (c) Adsorption energy contour on the Pd (1 1 1) surface. (For interpretation of the references to colour in this figure legend, the reader is referred to the web version of this article.)

tions, the strongest CO adsorption is on the Pd (1 1 1) three fold sites, at approximately 0.12 eV stronger than the most stable adsorption on Pt (1 1 1).

3.2. CO lateral interactions on Pt (1 1 1) vs Pd (1 1 1)

All DFT calculations show that CO molecules are almost perpendicular to surfaces with largest tilting angle around 3°, and no CO dimer is observed to form. LG model therefore can be expected to describe CO–CO interactions in good qualities. CO molecules on transition metal surfaces repulsively interact with each other, leading to a decreasing average binding energy as a function of coverage. Such trend has been observed both experimentally and through FP calculations [22,29,42]. Our previous study on CO lateral interactions on Pt (1 1 1) surface indicates that CO intermolecular interactions are of short range nature [22], thus we limit the range of the lattice gas model interaction up to a cut off distance of two lattice constants. For practical purpose, it was found that expansion up to two-body terms provides satisfactory accuracy for both low and high CO coverages on Pt (1 1 1) and Pd (1 1 1), with an average deviation of 15 meV per molecular CO adsorption. This is inline with other literature findings that pair-wise terms give reasonable accuracy in describing CO lateral interactions on transition metal surfaces [22,37,43]. Optimized lattice gas expansion coefficients on each metal contain 36 terms, each of which corresponds to a particular line pair as enumerated in Fig. 2a. FP calculations have demonstrated that if two CO molecules occupy two sites with distance smaller than one lattice constant, the system becomes unstable. Therefore, interactions of these pairs are artificially set to 20 eV in LG-MC to indicate the incompatibility of co-adsorption on these sites [43].

A detailed list of all the significant lattice gas interaction coefficients on Pt (1 1 1) and Pd (1 1 1) surfaces are enumerated in Tables 1 and 2, respectively. We can see some commonalities and differences of CO interactions on Pt (1 1 1) and Pd (1 1 1): (a) CO interactions on both Pt (1 1 1) and Pd (1 1 1) are repulsive, as illustrated by positive numbers in these two tables. The repulsion decreases with the increase of the intermolecular distance. (b) as far as onsite adsorption energies are concerned, CO adsorption is most stable at three fold sites on Pd (1 1 1) and are almost isoenergetic on Pt (1 1 1). This would have significant influence on the type of dominant CO interactions on the surface, as we expect more threefold CO adsorption on Pd (1 1 1) as compared to that on Pt (1 1 1). (c) The repulsion between adsorbed CO on two adjacent sites is larger when two CO molecules are at three fold sites as compared to CO molecules at atop sites. The H–H (1st NN) on Pd (1 1 1) is 288 meV, while A–A (1st NN) on the same surface is only 205 meV. This is due to the fact that two hcp adsorbed CO directly share a common metal atom on the surface, leading to an effective repulsion due to substrate-mediated metal sharing effect [22]. Since CO molecules

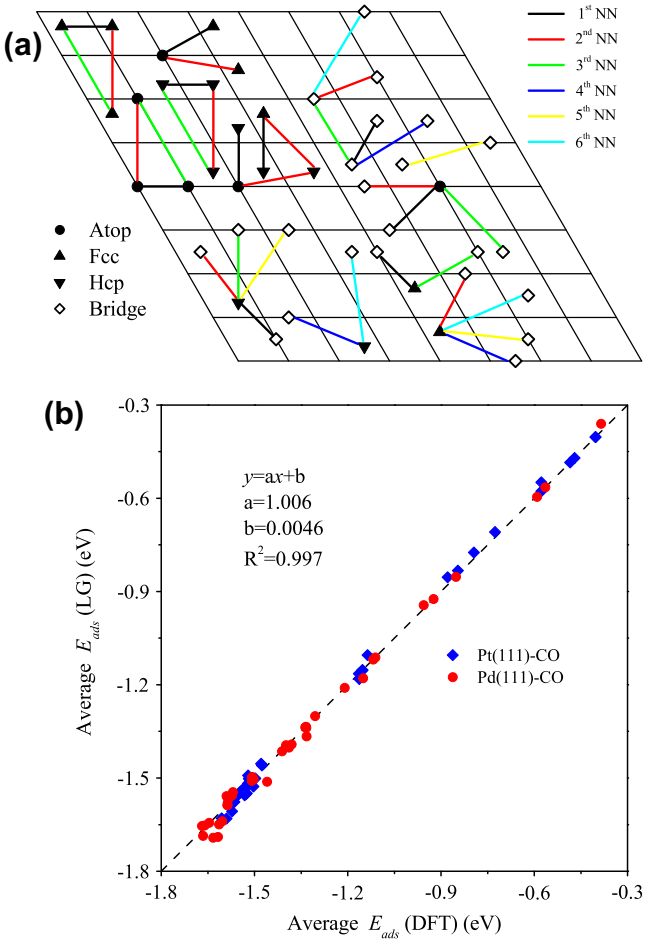

Fig. 2. (a) Illustration of lattice gas CO–CO pair interactions. Note that colors of connecting lines are sorted according to the *i*th nearest neighbor (NN) pair, not the distances. (b) Energy correlation between DFT and lattice gas model for 94 configurations. (For interpretation of the references to colour in this figure legend, the reader is referred to the web version of this article.)

prefer threefold adsorption on the Pd (1 1 1) surface, the effective lateral interactions between CO molecules are larger. This effect is best illustrated in the LG-MC simulation and the resulting differential adsorption energy curve that we will describe in the following section. Finally, we want to note that with a slope very close to 1.0, and square of the sample correlation coefficient (*R* squared value) of 0.997, our lattice gas parameters reliably reproduces CO adsorption energies across the 94 configurations considered at both low coverage and high coverage [Fig. 2b].

Table 1
Enumeration of lattice gas expansion coefficients for CO adsorption on the Pt (1 1 1) surface. A, H, F, and B are the same as in Fig. 1.

Clusters	Geometry ($/a_0$)	Pt (1 1 1) interaction (meV)	Clusters	Geometry ($/a_0$)	Interaction (meV)
A–A	1st-NN (1)	180.6	H–B	6th-NN $\left(\sqrt{\frac{43}{12}}\right)$	93.0
A–A	2nd-NN $\left(\sqrt{3}\right)$	95.1	F–F	1st-NN (1)	274.9
A–A	3rd-NN (2)	48.4	F–F	2nd-NN $\left(\sqrt{3}\right)$	58.9
A–H	1st-NN $\left(\frac{2\sqrt{3}}{3}\right)$	101.9	F–F	3rd-NN (2)	52.6
A–H	2nd-NN $\left(\sqrt{\frac{7}{3}}\right)$	92.3	F–B	1st-NN $\left(\sqrt{\frac{13}{12}}\right)$	225.9
A–F	1st-NN $\left(\frac{2\sqrt{3}}{3}\right)$	68.4	F–B	2nd-NN $\left(\sqrt{\frac{19}{12}}\right)$	149.1
A–F	2nd-NN $\left(\sqrt{\frac{7}{3}}\right)$	67.3	F–B	3rd-NN $\left(\sqrt{\frac{25}{12}}\right)$	118.3
A–B	1st-NN $\left(\frac{\sqrt{7}}{2}\right)$	97.3	F–B	4th-NN $\left(\sqrt{\frac{31}{12}}\right)$	100.8
A–B	2nd-NN $\left(\frac{3}{2}\right)$	100.8	F–B	5th-NN $\left(\sqrt{\frac{37}{12}}\right)$	110.3
A–B	3rd-NN $\left(\frac{\sqrt{13}}{2}\right)$	88.1	F–B	6th-NN $\left(\sqrt{\frac{43}{12}}\right)$	93.0
H–H	1st-NN (1)	305.7	B–B	1st-NN pair (1)	243.2
H–H	2nd-NN $\left(\sqrt{3}\right)$	69.5	B–B	2nd-NN $\left(\frac{\sqrt{7}}{2}\right)$	142.1
H–H	3rd-NN (2)	26.3	B–B	3rd-NN $\left(\frac{3}{2}\right)$	118.9
H–F	1st-NN $\left(\frac{2\sqrt{3}}{3}\right)$	133.5	B–B	4th-NN $\left(\sqrt{3}\right)$	105.4
H–F	2nd-NN $\left(\sqrt{\frac{7}{3}}\right)$	113.8	B–B	5th-NN $\left(\frac{\sqrt{13}}{2}\right)$	162.2
H–B	1st-NN $\left(\sqrt{\frac{13}{12}}\right)$	225.9	B–B	6th-NN (2)	33.5
H–B	2nd-NN $\left(\sqrt{\frac{19}{12}}\right)$	149.1	A	–	-1.550×10^3
H–B	3rd-NN $\left(\sqrt{\frac{25}{12}}\right)$	118.3	H	–	-1.607×10^3
H–B	4th-NN $\left(\sqrt{\frac{31}{12}}\right)$	100.8	F	–	-1.629×10^3
H–B	5th-NN $\left(\sqrt{\frac{37}{12}}\right)$	110.3	B	–	-1.631×10^3

Table 2
Enumeration of lattice gas expansion coefficients for CO adsorption on the Pd (1 1 1) surface. A, H, F, and B are the same as in Fig. 1.

Clusters	Geometry ($/a_0$)	Pd (1 1 1) interaction (meV)	Clusters	Geometry ($/a_0$)	Interaction (meV)
A–A	1st-NN (1)	205.4	H–B	6th-NN $\left(\sqrt{\frac{43}{12}}\right)$	62.4
A–A	2nd-NN $\left(\sqrt{3}\right)$	71.3	F–F	1st-NN (1)	270.2
A–A	3rd-NN (2)	28.5	F–F	2nd-NN $\left(\sqrt{3}\right)$	75.1
A–H	1st-NN $\left(\frac{2\sqrt{3}}{3}\right)$	121.3	F–F	3rd-NN (2)	17.7
A–H	2nd-NN $\left(\sqrt{\frac{7}{3}}\right)$	104.8	F–B	1st-NN $\left(\sqrt{\frac{13}{12}}\right)$	185.4
A–F	1st-NN $\left(\frac{2\sqrt{3}}{3}\right)$	102.4	F–B	2nd-NN $\left(\sqrt{\frac{19}{12}}\right)$	87.4
A–F	2nd-NN $\left(\sqrt{\frac{7}{3}}\right)$	78.1	F–B	3rd-NN $\left(\sqrt{\frac{25}{12}}\right)$	28.4
A–B	1st-NN $\left(\frac{\sqrt{7}}{2}\right)$	21.2	F–B	4th-NN $\left(\sqrt{\frac{31}{12}}\right)$	28.2
A–B	2nd-NN $\left(\frac{3}{2}\right)$	56.8	F–B	5th-NN $\left(\sqrt{\frac{37}{12}}\right)$	26.5
A–B	3rd-NN $\left(\frac{\sqrt{13}}{2}\right)$	53.5	F–B	6th-NN $\left(\sqrt{\frac{43}{12}}\right)$	62.4
H–H	1st-NN (1)	287.7	B–B	1st-NN pair (1)	235.3
H–H	2nd-NN $\left(\sqrt{3}\right)$	72.2	B–B	2nd-NN $\left(\frac{\sqrt{7}}{2}\right)$	9.9
H–H	3rd-NN (2)	15.2	B–B	3rd-NN $\left(\frac{3}{2}\right)$	17.8
H–F	1st-NN $\left(\frac{2\sqrt{3}}{3}\right)$	84.0	B–B	4th-NN $\left(\sqrt{3}\right)$	30.8
H–F	2nd-NN $\left(\sqrt{\frac{7}{3}}\right)$	23.0	B–B	5th-NN $\left(\frac{\sqrt{13}}{2}\right)$	7.6
H–B	1st-NN $\left(\sqrt{\frac{13}{12}}\right)$	185.4	B–B	6th-NN (2)	11.1
H–B	2nd-NN $\left(\sqrt{\frac{19}{12}}\right)$	87.4	A	–	-1.214×10^3
H–B	3rd-NN $\left(\sqrt{\frac{25}{12}}\right)$	28.4	H	–	-1.689×10^3
H–B	4th-NN $\left(\sqrt{\frac{31}{12}}\right)$	28.2	F	–	-1.692×10^3
H–B	5th-NN $\left(\sqrt{\frac{37}{12}}\right)$	26.5	B	–	-1.512×10^3

3.3. Monte-Carlo simulations of CO adsorption patterns and saturation coverage

To explore and compare CO adsorption characteristics on Pt (1 1 1) and Pd (1 1 1) surfaces, we carried out LG-MC simulations on a 12×12 unit cell with periodic boundary condition at a temperature of 70 K. Fig. 3 shows adsorption energy curves for nCO molecules on Pt (1 1 1) and Pd (1 1 1) from LG-MC simulations, where n equals the number of surface metal atoms times coverage. At low coverage, CO molecules tend to deposit onto the Pt (1 1 1) and the Pd (1 1 1) surfaces since E_{ads} is negative and lower than the chemical potential of CO in the gas phase. As the coverage increases, adsorption of CO molecules becomes less energetically favorable because of the repulsive CO–CO lateral interactions. We note that even under the limit of zero kelvin and high CO pressure, the lateral interactions among CO molecules prevent the full monolayer passivation of either Pt (1 1 1) or Pd (1 1 1). The lowest total system energy on the Pt (1 1 1) surface appears at 0.75 ML while that on the Pd (1 1 1) surface shows around 0.70 ML. To discuss the total energy curve more quantitatively, we also present Hull curves of these two surfaces, shown as red solid lines in Fig. 3a and b, respectively. The Hull curve is a convex polyline within the whole range of the coverage, with its vertexes corresponding to all the true ground configurations [44]. As shown in Fig. 3a and b, up to 0.75 ML, the LG-MC simulations identify all the vertexes, which demonstrates the reliability of our results. The only deviation from the Hull curve of the Pt (1 1 1) surface happens at 0.90 ML, which decomposes, at least in principle, into a mixture of 0.80 ML and 1.00 ML. Similar discussions can be made for the Pd (1 1 1) surface, in which case 0.95 ML is unstable and tends to decompose into a mixture of 0.90 ML and 1.00 ML. However, these high coverages are not accessible according to the total energy curve and the deviations does not influence our discussion of the CO adsorption behavior under realistic reacting conditions.

One can also calculate the average chemical potential of a CO molecule from the derivative of the Hull curves with respect to the coverage:

$$\mu_{CO}(\theta) = \frac{\partial E_{ads}(\theta)}{\partial \theta}, \tag{3}$$

where $\mu_{CO}(\theta)$ is the chemical potential and indicates to what extent a CO molecule tends to adsorb onto the surface at a given coverage. The results are shown in Fig. 3c. $\mu_{CO}(\theta)$ increases monotonically with the increase of coverage, which means the tendency of adsorption of a CO molecule keeps being weakened by the lateral interactions. Especially, $\mu_{CO}(\theta)$s of the Pt (1 1 1) surface and the Pd (1 1 1) surface change signs at 0.75 ML and 0.70 ML, respectively. Correspondingly, the saturation coverage on Pt (1 1 1) is close to 0.75 ML while that on Pd (1 1 1) is at a lower threshold of 0.70 ML. One should note, furthermore, that $\mu_{CO}(\theta)$ of the Pd (1 1 1) surface increases faster than that of the Pt (1 1 1) surface and the crossing happens at 0.50 ML. Consequently, CO molecular desorption takes less energy to happen on Pd (1 1 1) surface with $\theta \geqslant 0.5$ML. These two points indicate that Pd (1 1 1) could potentially be a more reactive surface towards CO oxidation under low temperatures, since it has both a lower CO desorption energy and a potentially lower oxygen dissociation barrier due to lower CO covearge [23].

Kinks of the $\mu_{CO}(\theta)$ curve indicate change of configurations for the CO-adsorbed surfaces. In order to investigate the change of the adsorption pattern as a function of the coverage in detail, we show snapshots of the MC configuration under equilibrium in Fig. 4. On the Pt (1 1 1) surface, CO molecules randomly deposit on the bridge sites up to 0.15 ML, beyond which ordered pattern gradually appears due to the lateral interactions. As shown in Fig. 4a, a $c(4 \times 2\sqrt{3})$-3CO super-structure gradually shows up until 0.35 ML. As the coverage increases further, the pattern begins to transfer. Consequently, adsorbed CO molecules show less ordered structures in the range of 0.40 ML to 0.50 ML. From 0.55 ML, the CO-decorated Pt (1 1 1) surface shows a $p(3 \times 3)$ super-structure, which is most clear at 0.75 ML as $p(3 \times 3)$-7CO. This structure corresponds the most stable configurations since if more CO molecules adsorb to the surface, H–H (1st NN) and F–F (1st NN) interactions overcompensate the energetic gain due to the adsorption and therefore reverse the sign of μ_{CO}. On the Pd (1 1 1) surface, CO molecules do not show any ordered structure up to 0.20 ML, which is similar to the case of the Pt (1 1 1) surface. Beyond 0.20 ML, lateral interactions affect the distribution of CO molecules and the system shows partially ordered structure in certain snapshots of MC. As the coverage increases further, the surface begins to show a $p(2 \times 2)$-2CO reconstruction, as shown in Fig. 4b at 0.45 ML. Beyond 0.50 ML, however, the ordering of the adsorbed CO molecules becomes blur very quickly and no clear patterns were identified at higher coverages [Fig. 4b].

One should note that on the Pd (1 1 1) surface, CO molecules mainly deposit onto threefold hollow sites even at very high coverage. In contrast, CO molecular adsorption consists of a mix of atop, hcc and fcc sites to minimize the repulsive lateral interactions on the Pt (1 1 1) surface. This difference is a reflection of the adsorption energy differences shown in Fig. 1b and c contour plots. On the Pd (1 1 1) surface, the difference of E_{ads} at atop and fcc sites is around 0.5 eV, while it is less than 0.1 eV on the Pt (1 1 1) surface. Such differences leads to more threefold populated adsorption configurations for CO on Pd (1 1 1) and more H–H (1st NN) and F–F (1st NN) interactions. Based on the parameters in Tables 1 and 2, we

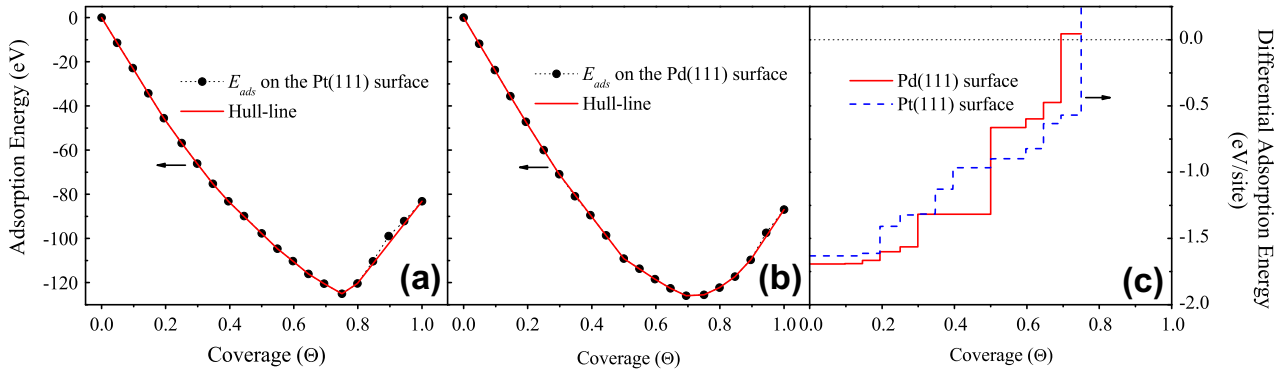

Fig. 3. Total adsorption energy of the system as a function of CO coverage for (a) Pt (1 1 1) and (b) Pd (1 1 1). (c) Differential binding energy curve of CO on Pt (1 1 1) and Pd (1 1 1).

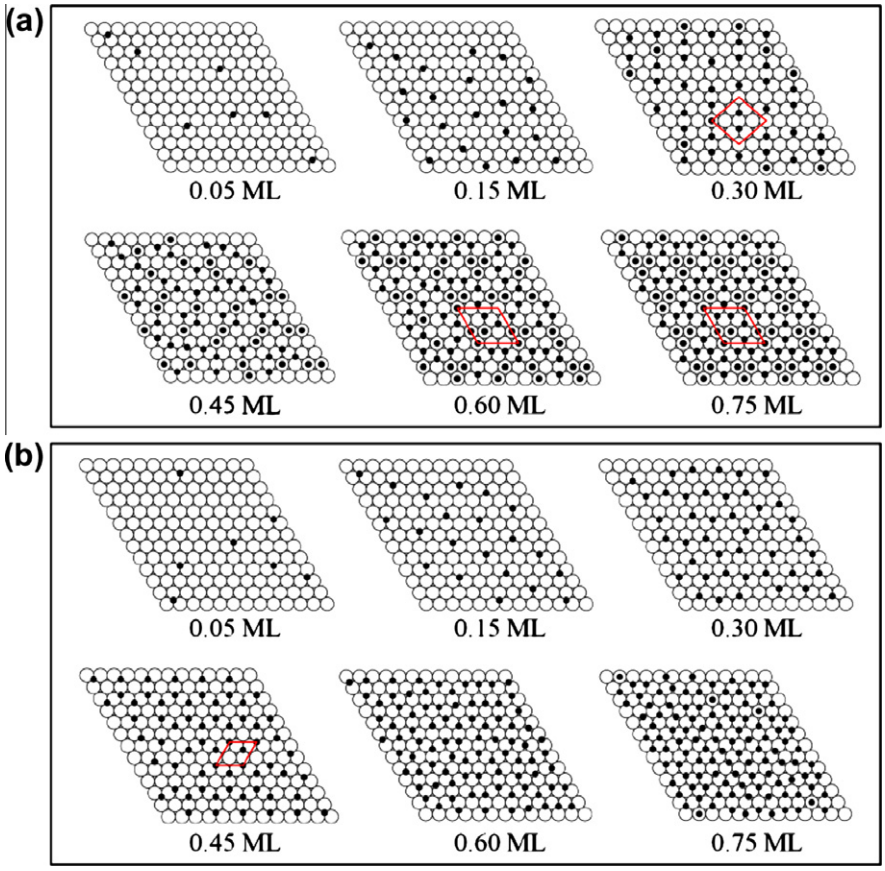

Fig. 4. CO equilibrium adsorption geometries from LG-MC simulations for coverages of 0.05 ML, 0.15 ML, 0.30 ML, 0.45 ML, 0.60 ML, and 0.75 ML on (a) Pt (1 1 1) and (b) Pd (1 1 1) surfaces, respectively. Red cells indicate possible super-structures observed during MC simulations. (For interpretation of the references to color in this figure legend, the reader is referred to the web version of this article.)

can see that these two interactions are the main contributions leading to the weakening of the μ_{CO}. Consequently, one can expect that μ_{CO} should be weakened faster on the Pd (1 1 1) surface and a lower saturation coverage ensues, despite its stronger CO adsorption energy in low coverage limit.

4. Conclusions

We investigated in detail the CO adsorption on Pt (1 1 1) and Pd (1 1 1) using a first-principles based lattice gas Monte-Carlo simulation. It is shown that differential adsorption energy curve is a combined result of CO onsite binding and CO lateral repulsions. While CO binds stronger on Pd (1 1 1) at low coverage, the stronger repulsion between neighboring threefold sites leads to a more rapid decrease in binding energy on Pd (1 1 1). The resulting lower saturation coverage of CO and lower CO binding energies could contribute to the excellent reactivity observed on Pd surfaces. Our results signify the importance of CO lateral interactions and give insight into the CO oxidation reaction on transition metal surfaces under high pressure conditions.

Acknowledgements

This work is supported by the Program for Changjiang Scholars and Innovative Research Team in University (PCSIRT) and National Natural Science Foundation of China (11004068). R. Chen and B. Shan would like to acknowledge the support from the Program for New Century Excellent Talents in University (NCET). Calculations presented in this paper were carried out using the High Performance Computing Center experimental testbed in SCTS/CGCL (see http://grid.hust.edu.cn/hpcc)

References

[1] J. Despres, M. Elsener, M. Koebel, O. Krocher, B. Schnyder, A. Wokaun, Catalytic oxidation of nitrogen monoxide over Pt/SiO_2, Applied Catalysis B – Environmental 50 (2) (2004) 73–82.
[2] C.H. Kim, G. Qi, K. Dahlberg, W. Li, Strontium-doped perovskites rival platinum catalysts for treating NO_x in simulated diesel exhaust, Science 327 (5973) (2010) 1624–1627.
[3] R. Kissel-Osterrieder, F. Behrendt, J. Warnatz, U. Metka, H.-R. Volpp, J. Wolfrum, Experimental and theoretical investigation of co oxidation on platinum: bridging the pressure and materials gap, Proceedings of the Combustion Institute 28 (1) (2000) 1341–1348.
[4] V. Zhdanov, B. Kasemo, Steady-state kinetics of co oxidation on Pt: extrapolation from 10^{-10} to 1 bar, Applied Surface Science 74 (2) (1994) 147–164.
[5] D.J. Burnett, A.T. Capitano, A.M. Gabelnick, A.L. Marsh, D.A. Fischer, J.L. Gland, In-situ soft X-ray studies of co oxidation on the Pt(111) surface, Surface Science 564 (1–3) (2004) 29–37.
[6] A.K. Santra, D.W. Goodman, Catalytic oxidation of CO by platinum group metals: from ultrahigh vacuum to elevated pressures, Electrochimica Acta 47 (22–23) (2002) 3595–3609.
[7] X. Hao, B. Shan, J. Hyun, N. Kapur, K. Fujdala, T. Truex, K. Cho, Experimental and theoretical study of CO oxidation on PdAu catalysts with NO pulse effects, Topics in Catalysis 52 (13–20) (2009) 1946–1950.
[8] B. Shan, L. Wang, S. Yang, J. Hyun, N. Kapur, Y. Zhao, J.B. Nicholas, K. Cho, First-principles-based embedded atom method for PdAu nanoparticles, Physical Review B 80 (3) (2009) 035404.
[9] J. Wintterlin, S. Volkening, T. Janssens, T. Zambelli, G. Ertl, Atomic and macroscopic reaction rates of a surface-catalyzed reaction, Science 278 (5345) (1997) 1931–1934.
[10] M. Valden, X. Lai, D.W. Goodman, Onset of catalytic activity of gold clusters on titania with the appearance of nonmetallic properties, Science 281 (5383) (1998) 1647–1650.
[11] P.J. Berlowitz, C.H.F. Peden, D.W. Goodman, Kinetics of CO oxidation on single-crystal Pd, Pt, and Ir., Journal of Physical Chemistry 92 (18) (1988) 5213–5221.

[12] D. Burnett, A. Capitano, A. Gabelnick, A. Marsh, D. Fischer, J. Gland, In-situ soft X-ray studies of CO oxidation on the Pt(1 1 1) surface, Surface Science 564 (1–3) (2004) 29–37.
[13] H. Steininger, S. Lehwald, H. Ibach, On the adsorption of CO on Pt(1 1 1), Surface Science 123 (2–3) (1982) 264–282.
[14] G. Ertl, M. Neumann, K. Streit, Chemisorption of CO on Pt(1 1 1) surface, Surface Science 64 (2) (1977) 393–410.
[15] B. Persson, M. Tushaus, A. Bradshaw, On the nature of dense CO adlayers, Journal of Chemical Physics 92 (8) (1990) 5034–5046.
[16] H. Steininger, S. Lehwald, H. Ibach, On the adsorption of CO on Pt(1 1 1), Surface Science 123 (2–3) (1982) 264–282.
[17] E. Vestergaard, P. Thostrup, T. An, E. Laegsgaards, I. Stensgaard, B. Hammer, F. Besenbacher, Comment on high pressure adsorbate structures studied by scanning tunneling microscopy: CO on Pt(1 1 1) in equilibrium with the gas phase, Physical Review Letters 88 (25) (2002) 259601/1.
[18] S.R. Longwitz, J. Schnadt, E.K. Vestergaard, R.T. Vang, E. Laegsgaard, I. Stensgaard, H. Brune, F. Besenbacher, High-coverage structures of carbon monoxide adsorbed on Pt(1 1 1) studied by high-pressure scanning tunneling microscopy, Journal of Physical Chemistry B 108 (38) (2004) 14497–14502.
[19] Y.T. Wong, R. Hoffmann, Chemisorption of carbon monoxide on three metal surfaces: Ni(1 1 1), Pd(1 1 1), and Pt(1 1 1). a comparative study, Journal of Physical Chemistry 95 (2) (1991) 859–867.
[20] H. Yang, J.F. Sanz, Y. Wang, J.L. Whitten, Adsorption energetics of NO and CO on Pt(1 1 1), Journal of Cluster Science 10 (4) (1999) 581–590.
[21] J. Steckel, A. Eichler, J. Hafner, CO adsorption on the CO-precovered Pt(1 1 1) surface characterized by density-functional theory, Physical Review B 68 (8) (2003) 085416.
[22] B. Shan, Y. Zhao, J. Hyun, N. Kapur, J.B. Nicholas, K. Cho, Coverage-dependent CO adsorption energy from first-principles calculations, The Journal of Physical Chemistry C 113 (15) (2009) 6088–6092.
[23] B. Shan, N. Kapur, J. Hyun, L. Wang, J.B. Nicholas, K. Cho, CO-coverage-dependent oxygen dissociation on Pt(1 1 1) surface, The Journal of Physical Chemistry C 113 (2) (2009) 710–715.
[24] C. Campell, G. Ertl, H. Kuipers, J. Segner, A molecular beam study of the catalytic oxidation of CO on a Pt(1 1 1)surface, Journal of Chemical Physics 73 (11) (1980) 5862–5873.
[25] T. Bunluesin, E. Putna, R. Gorte, A comparison of CO oxidation on ceria-supported Pt, Pd, and Rh, Catalysis Letters 41 (1–2) (1996) 1–5.
[26] G. Kresse, J. Furthmuller, Efficiency of ab-initio total energy calculations for metals and semiconductors using a plane-wave basis set, Computational Materials Science 6 (1) (1996) 15–50.
[27] P. Blochl, Projector augmented-wave method, Physical Review B 50 (24) (1994) 17953–17979.
[28] J.P. Perdew, K. Burke, M. Ernzerhof, Generalized gradient approximation made simple, Physical Review Letters 77 (18) (1996) 3865–3868.
[29] M. Gajdos, A. Eichler, J. Hafner, CO adsorption on close-packed transition and noble metal surfaces: trends from ab initio calculations, Journal of Physics Condensed Matter 16 (8) (2004) 1141–1164.
[30] G. Kresse, A. Gil, P. Sautet, Significance of single-electron energies for the description of CO on Pt(1 1 1), Physical Review B 68 (7) (2003). 73401-1–4.
[31] P. Feibelman, B. Hammer, J. Norskov, F. Wagner, M. Scheffler, R. Stumpf, R. Watwe, J. Dumesic, The CO/Pt(1 1 1) puzzle, Journal of Physical Chemistry B 105 (18) (2001) 4018–4025.
[32] A. Gil, A. Clotet, J.M. Ricart, G. Kresse, M. Garcia-Hernandez, N. Rosch, P. Sautet, Site preference of co chemisorbed on Pt(1 1 1) from density functional calculations, Surface Science 530 (1–2) (2003) 71–86.
[33] L.C. Grabow, A.A. Gokhale, S.T. Evans, J.A. Dumesic, M. Mavrikakis, Mechanism of the water gas shift reaction on Pt: first principles, experiments, and microkinetic modeling, The Journal of Physical Chemistry C 112 (12) (2008) 4608–4617.
[34] D. Ford, Y. Xu, M. Mavrikakis, Atomic and molecular adsorption on Pt(1 1 1), Surface Science 587 (3) (2005) 159–174.
[35] B.C. Han, A. Van der Ven, G. Ceder, B.-J. Hwang, Surface segregation and ordering of alloy surfaces in the presence of adsorbates, Physical Review B 72 (20) (2005) 205409.
[36] A. van de Walle, G. Ceder, The effect of lattice vibrations on substitutional alloy thermodynamics, Review of Modern Physics 74 (1) (2002) 11–45.
[37] D. Liu, Lattice-gas modeling of CO adlayers on Pd(1 0 0), Journal of Chemical Physics 121 (9) (2004) 4352–4357.
[38] N. Metropolis, A.W. Rosenbluth, M.N. Rosenbluth, A.H. Teller, E. Teller, Equation of state calculations by fast computing machines, Journal of Chemical Physics 21 (1953) 1087–1092.
[39] S. Kirkpatrick, C. Gelatt, M. Vecchi, Optimization by simulated annealing, Science 220 (4598) (1983) 671–680.
[40] C. Zhang, P. Hu, A. Alavi, A general mechanism for co oxidation on close-packed transition metal surfaces, Journal of the American Chemical Society 121 (34) (1999) 7931–7932.
[41] C.J. Zhang, P. Hu, CO oxidation on Pd(1 0 0) and Pd(1 1 1): a comparative study of reaction pathways and reactivity at low and medium coverages, Journal of the American Chemical Society 123 (6) (2001) 1166–1172.
[42] Y. Yeo, L. Vattuone, D. King, Calorimetric heats for co and oxygen adsorption and for the catalytic co oxidation reaction on Pt{1 1 1}, Journal of Chemical Physics 106 (1) (1997) 392–401.
[43] K. Honkala, P. Pirilä, K. Laasonen, Coadsorption of CO and NO on the Pd(1 1 1) surface: combined ab initio and Monte Carlo study, Physical Review Letters 86 (26) (2001) 5942–5945.
[44] R.B. Getman, Y. Xu, W.F. Schneider, Thermodynamics of environment-dependent oxygen chemisorption on Pt(1 1 1), The Journal of Physical Chemistry C 112 (26) (2008) 9559–9572.